Separation Science and Technology
Publication details, including instructions for authors and subscription information:
http://www.informaworld.com/smpp/title~content=t713708471

Effect of Membrane Structural Characteristics on Mass Transfer in a Membrane Absorption Process

Weidong Zhang[a]; Geng Chen[a]; Wei Sun[a]; Jiang Li[a]
[a] State Key Laboratory of Chemical Resource Engineering, Beijing University of Chemical Technology, Beijing, People's Republic of China

Online publication date: 02 June 2010

To cite this Article Zhang, Weidong , Chen, Geng , Sun, Wei and Li, Jiang(2010) 'Effect of Membrane Structural Characteristics on Mass Transfer in a Membrane Absorption Process', Separation Science and Technology, 45: 9, 1216 — 1227
To link to this Article: DOI: 10.1080/01496391003775816
URL: http://dx.doi.org/10.1080/01496391003775816

Separation Science and Technology, 45: 1216–1227, 2010

ISSN: 0149-6395 print/1520-5754 online
DOI: 10.1080/01496391003775816

Taylor & Francis
Taylor & Francis Group

Effect of Membrane Structural Characteristics on Mass Transfer in a Membrane Absorption Process

Weidong Zhang, Geng Chen, Wei Sun, and Jiang Li
State Key Laboratory of Chemical Resource Engineering, Beijing University of Chemical Technology, Beijing, People's Republic of China

Carbon dioxide is absorbed by de-ionized water or NaOH aqueous solution in the unsteady-state membrane absorption process. A theoretical model has been developed to describe the mass transfer behavior in the liquid phase, in which the effects of membrane structural characteristics are investigated. The concentration profiles in the liquid phase are calculated as a function of time. When the membrane porosity is relatively high or the pore size is relatively small, the solute concentration profile near the membrane surface can get homogeneous instantly due to the short distance between adjacent pores. In this case, the existence of the porous membrane has less effect on the mass transfer process. However, when the membrane porosity is relatively low or the pore size is relatively large, the distance between the adjacent pores is large, so the concentration profile near the membrane surface is hard to get homogeneous during the absorption process. Therefore, the concentration profile can be influenced significantly by the membrane structural characteristics, which means that the membrane structure has a significant effect on the mass transfer in liquid phase. Moreover, the chemical reaction in the liquid phase makes it difficult for the concentration profile near the membrane surface to get homogeneous. The disturbance in the liquid phase caused by the gas flow and pressure fluctuation is also taken into account in the model, and the model results agree well with the experimental data.

Keywords gas absorption; mass transfer; porous membrane; structural characteristics; theoretical model

INTRODUCTION

Global warming, a consequence of the enhanced greenhouse effect caused by human activities, has become one of the key climate problems all over the world. Among all the greenhouse gases, carbon dioxide (CO_2) is expected to play the most important role (1). Separation and capture of CO_2 can help slow down the greenhouse effect development efficiently.

In the membrane absorption process, gas and liquid flows are handled separately; the mass transfer area in a unit space is relatively larger than other separation techniques; and it is easy to scale up. All these advantages make it one of the most promising alternatives for CO_2 capture (2,3).

Membrane absorption technology was originated by Zhang Qi and Cussler in 1985 (4,5). Since then, large numbers of researches on the membrane absorption process have been done (6–14). In the membrane absorption process, micro-porous membranes are applied. The interfacial mass transfer between the gas and liquid phases occurs only at the pores on the membrane surface. The membrane body just provides a support. The solute cannot diffuse through the membrane body (15). Therefore, the existence of the porous membrane can affect the concentration profile in the liquid phase. Membrane porosity and pore size all have an impact on the effective mass transfer area.

In some other membrane processes, the effect of the membrane structure characteristics on the mass transfer in the liquid phase has been studied (16–18). However, it is neglected in the membrane absorption processes. Membrane structural characteristics are generally considered to affect the membrane resistance merely. Most researchers take the whole membrane surface area or the overall pore area as the effective mass transfer area (19–22). Kreulen et al. (23) studied the CO_2 absorption process using de-ionized water in a hollow fiber contactor. According to their conclusions, the whole membrane area should be used as a mass transfer area, and the membrane porosity had no effect on mass transfer. And the whole membrane area was used as the mass transfer area in many other researches (15,24,25). On the contrary, Kim and Yang (11) deemed that the membrane porosity had a significant effect on the mass transfer performance, and the effective mass transfer area should be the pore area of the membrane. Huseni and Rangwala (26) used a hollow fiber membrane with the porosity of 30% to absorb CO_2, and elicited that the ratio of the effective mass transfer area to the whole membrane area was 0.58, which means that the effective mass transfer area is neither the total area of the pores nor the membrane surface area.

In our previous research (27,28), it was found that membrane porosity had little effect on the mass transfer

Received 19 March 2009; accepted 16 February 2010.
Address correspondence to Wei Sun, College of Chemical Engineering, Beijing University of Chemical Technology, PO Box 1#, Beijing 100029, PR China. E-mail: sunwei@mail.buct.edu.cn

for the CO_2-water system, but had a significant effect for CO_2-NaOH aqueous solution system. A theoretical model based on the advancing front model was developed to analyze the effect of membrane structural characteristics in the unsteady-state mass transfer process (29). However, it is very difficult to simulate the mass transfer process when reaction fronts are overlapped, so that the applicability of this model is limited.

In this work, a theoretical model is developed to describe the effect of membrane structural characteristics on the mass transfer in the liquid phase. The membrane porosity, pore radius, and the absorbent pH value are all considered in the model. The disturbance in the liquid phase caused by the gas flow and pressure fluctuation is also incorporated in the model. By analyzing the model, the effect of membrane structural characteristics and the mechanism of the effect can be interpreted.

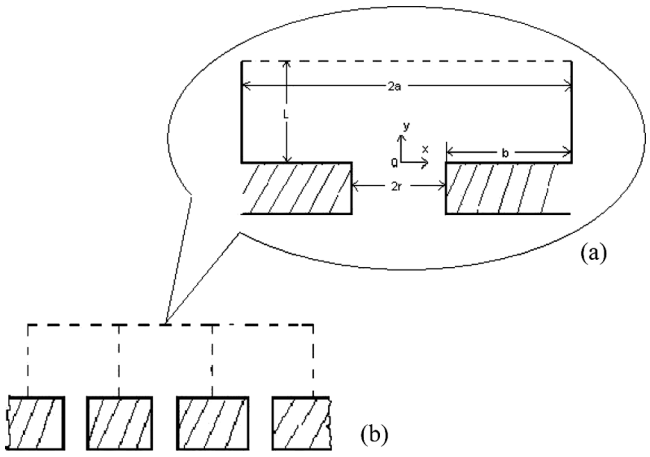

FIG. 1. Schematic representation of the membrane structure.

THEORY

Model Development

The aim is to describe the absorption of CO_2 into de-ionized water or NaOH solution, where the flat membranes are employed in this work. Both the gas phase and liquid phase are stagnant, so that the influence of the liquid flow can be avoided. As the absorption process is an unsteady-state process, the solute concentration profile in the liquid phase is a function of time.

To focus on the mass transfer in the liquid phase, the gas phase is pure CO_2 and the gas pressure is maintained constant. It is assumed that the micro-pores are not wetted under appropriate gas pressure. Therefore, the mass transfer resistances of the gas phase and membrane phase can be neglected. And the effect of the membrane thickness can be neglected too. The CO_2 concentration at the gas/liquid interface is assumed to follow Henry's law $c^* = \mathrm{pH}$. The Henry's law coefficient and diffusion coefficient are considered to be constant during the absorption process.

For simplicity, the structure of micro-porous membranes is assumed as repeats of one pore and one polymeric body with an invariant size, which is shown in Fig. 1. The membrane cross-sectional microstructure is assumed as straight through pores, since the mass transfer resistance in the membrane phase can be neglected, and therefore the tortuous pore structure has little effect on the mass transfer process in this work.

Mass Transfer with Chemical Reaction

When NaOH aqueous solutions are used as absorbents, the CO_2 and OH^- concentration above a pore in the liquid phase can be predicted by Eqs. (1) and (2) respectively.

$$\frac{\partial c_A}{\partial t} = D_A \frac{\partial^2 c_A}{\partial x^2} + D_A \frac{\partial^2 c_A}{\partial y^2} + R_A \tag{1}$$

$$\frac{\partial c_B}{\partial t} = D_B \frac{\partial^2 c_B}{\partial x^2} + D_B \frac{\partial^2 c_B}{\partial y^2} + R_B \tag{2}$$

where the subscripts A and B denote CO_2 and OH^-, respectively.

As the concentration profile is symmetric above a pore, half of the liquid region above a pore is considered. The initial and boundary conditions are:

$$t = 0,\ c_A = c_A^0,\ c_B = c_B^0$$

$$\begin{aligned}
&y = 0,\ 0 \le x \le r && c_A = c_A^*,\ \frac{\partial c_B}{\partial y} = 0 \\
&y = 0,\ r \le x \le a && \frac{\partial c_A}{\partial y} = 0,\ \frac{\partial c_B}{\partial y} = 0 \\
&x = 0,\ 0 \le y \le L && \frac{\partial c_A}{\partial x} = 0,\ \frac{\partial c_B}{\partial x} = 0 \\
&x = a,\ 0 \le y \le L && \frac{\partial c_A}{\partial x} = 0,\ \frac{\partial c_B}{\partial x} = 0 \\
&y = L,\ 0 \le x \le a && \frac{\partial c_A}{\partial y} = 0,\ \frac{\partial c_B}{\partial y} = 0
\end{aligned}$$

where R_A and R_B are reaction rates of CO_2 and OH^- respectively, L is the thickness of the liquid phase, c_A^0 and c_B^0 are the initial concentrations of CO_2 and OH^- in the liquid phase.

The reaction between CO_2 and OH^- can be represented as two steps:

$$CO_2 + OH^- \xrightarrow{k_1} HCO_3^- \tag{3}$$

$$HCO_3^- + OH^- \xrightarrow{k_2} CO_3^{2-} + H_2O \tag{4}$$

The reaction rate between CO_2 and OH^- can be calculated by Eqs. (5) and (6):

$$R_A = -k_1 C_A C_B \tag{5a}$$
$$R_B = -k_1 C_A C_B - k_2 C_B C_C \tag{5b}$$

where the subscript C denotes HCO_3^-, k_1 and k_2 are the forward rate constants of the first step and the second step reactions respectively.

Because the reaction rate constant of the second step is much larger than that of the first step ($k_2 \gg k_1$) (30–32), it can be concluded that there is no accumulation of HCO_3^- ions.

$$\frac{dC_C}{dt} = k_1 C_A C_B - k_2 C_B C_C = 0 \tag{6}$$

Substituting Eq. (6) into Eqs. (5b), (7) is obtained.

$$R_B = -2k_1 C_A C_B \tag{7}$$

Physical Mass Transfer Process

When de-ionized water is used as an absorbent, only physical absorption occurs. CO_2 concentration in the liquid phase can be predicted by Eq. (8).

$$\frac{\partial c_A}{\partial t} = D_A \frac{\partial^2 c_A}{\partial x^2} + D_A \frac{\partial^2 c_A}{\partial y^2} \tag{8}$$

The initial and boundary conditions are:

$$t = 0,\ c_A = c_A^0$$

$$\begin{aligned}
&y = 0,\ 0 \le x \le r && c_A = c_A^* \\
&y = 0,\ r \le x \le a && \frac{\partial c_A}{\partial y} = 0 \\
&x = 0,\ 0 \le y \le L && \frac{\partial c_A}{\partial x} = 0 \\
&x = a,\ 0 \le y \le L && \frac{\partial c_A}{\partial x} = 0 \\
&y = L,\ 0 \le x \le a && \frac{\partial c_A}{\partial y} = 0
\end{aligned}$$

Numerical Solution

The finite volume method (33) is applied to solve the set of partial differential equations listed above.

A portion of the interior grid used for the discretization is shown in Fig. 2. Integrating Eq. (1) over the control volume around node P and the time interval from t to $t+\Delta t$, Eq. (9) are obtained.

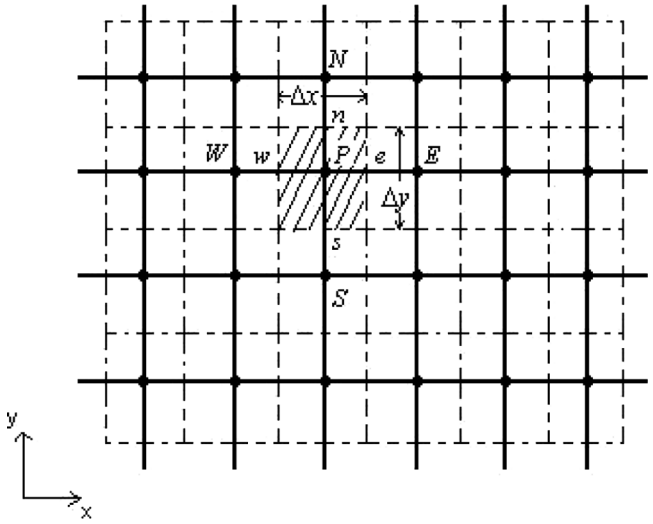

FIG. 2. Discretisation scheme of the interior grid.

$$\int_t^{t+\Delta t}\left[\int_{\Delta V}\left(\frac{\partial c_A}{\partial t}\right)dV\right]dt = \int_t^{t+\Delta t}\left[\int_{\Delta V}\frac{\partial}{\partial x}\left(D_A\frac{\partial c_A}{\partial x}\right)dV\right]dt + \int_t^{t+\Delta t}\left[\int_{\Delta V}\frac{\partial}{\partial y}\left(D_A\frac{\partial c_A}{\partial y}\right)dV\right]dt + \int_t^{t+\Delta t}\left(\int_{\Delta V} R_A dV\right)dt \tag{9}$$

According to Gauss' divergence theorem (33), the volume integrals in Eq. (9) can be changed to integrals over the entire bounding surface of the control volume.

Then Eq. (10) can be obtained.

$$\begin{aligned}
&\int_{\Delta V}\left[\int_t^{t+\Delta t}\left(\frac{\partial c_A}{\partial t}\right)dt\right]dV \\
&= \int_t^{t+\Delta t}\left[\left(D_A\frac{\partial c_A}{\partial x}A\right)_e - \left(D_A\frac{\partial c_A}{\partial x}A\right)_w\right]dt \\
&\quad + \int_t^{t+\Delta t}\left[\left(D_A\frac{\partial c_A}{\partial y}A\right)_n - \left(D_A\frac{\partial c_A}{\partial y}A\right)_s\right]dt \\
&\quad + \int_t^{t+\Delta t}\left(\int_{\Delta V} R_A dV\right)dt
\end{aligned} \tag{10}$$

where w, e, s, and n represent the bounding surfaces of the control volume.

The nonlinear reaction term is then pseudo-linearized by using Eq. (11).

$$R_A = -k_1 c_{B,P}^* c_{A,P} \tag{11}$$

where $c_{B,P}^*$ is the value of OH^- concentration from the previous iteration.

Assuming that a linear relationship between the concentration at the node P and those at its surrounding nodes, using a first order backward differencing scheme to replace

the time-dependent term $\partial c_A/\partial t$, and noting that $A_w = A_e = \Delta y$ and $A_s = A_n = \Delta x$, Eq. (10) can be approximated as:

$$\begin{aligned}(c_{A,P} - c^0_{A,P})\Delta x\Delta y &= \int_t^{t+\Delta t}\left[D_A\Delta x\left(\frac{c_{A,N}-c_{A,P}}{\delta y_{PN}} - \frac{c_{A,P}-c_{A,S}}{\delta y_{SP}}\right)\right]dt \\ &+ \int_t^{t+\Delta t}\left[D_A\Delta y\left(\frac{c_{A,E}-c_{A,P}}{\delta x_{PE}} - \frac{c_{A,P}-c_{A,W}}{\delta x_{WP}}\right)\right]dt \\ &- \int_t^{t+\Delta t}(-k_1 c^*_{B,P}c_{A,P}\Delta x\Delta y)dt \end{aligned} \quad (12)$$

where $c^0_{A,P}$ is the concentration (at node P) at the time t and $c_{A,P}$ is the concentration at the time $t+\Delta t$.

In order to evaluate the time integrals in Eq. (13), the fully implicit scheme is applied, and Eq. (13) is obtained.

$$\begin{aligned}\frac{c_{A,P}-c^0_{A,P}}{\Delta t}\Delta x\Delta y &= D_A\Delta x\left(\frac{c_{A,N}-c_{A,P}}{\delta y_{PN}} - \frac{c_{A,P}-c_{A,S}}{\delta y_{SP}}\right) \\ &+ D_A\Delta y\left(\frac{c_{A,E}-c_{A,P}}{\delta x_{PE}} - \frac{c_{A,P}-c_{A,W}}{\delta x_{WP}}\right) \\ &- kc^*_{B,P}c_{A,P}\Delta x\Delta y \end{aligned} \quad (13)$$

Re-range Eq. (13) in terms of concentrations at different nodes:

$$a_P c_{A,P} = a_W c_{A,W} + a_E c_{A,E} + a_S c_{A,S} + a_N c_{A,N} + a^0_P c^0_{A,P} \quad (14)$$

where

$$a_W = \frac{D_A\Delta y}{\delta x_{WP}},\ a_E = \frac{D_A\Delta y}{\delta x_{PE}},\ a_S = \frac{D_A\Delta x}{\delta y_{SP}},\ a_N = \frac{D_A\Delta x}{\delta y_{PN}}$$
$$a^0_P = \frac{\Delta x\Delta y}{\Delta t},\ S_P = -kc^*_{B,P}\Delta x\Delta y$$
$$a_P = a^0_P + a_W + a_E + a_S + a_N - S_P$$

Similarly, the discretized equations for component B could be yielded by pseudo-linearizing the reaction term as $\overline{R_B} = -k_1 c^*_{A,P}c_{B,P}$, where $c^*_{A,P}$ is the value obtained from the previous iteration.

When CO_2 is absorbed by de-ionized water, there is no reaction term since the chemical reaction between CO_2 and H_2O is neglected. Hence there is only one set of equations.

The algorithm for solving the sets of equations is shown in Fig. 3.

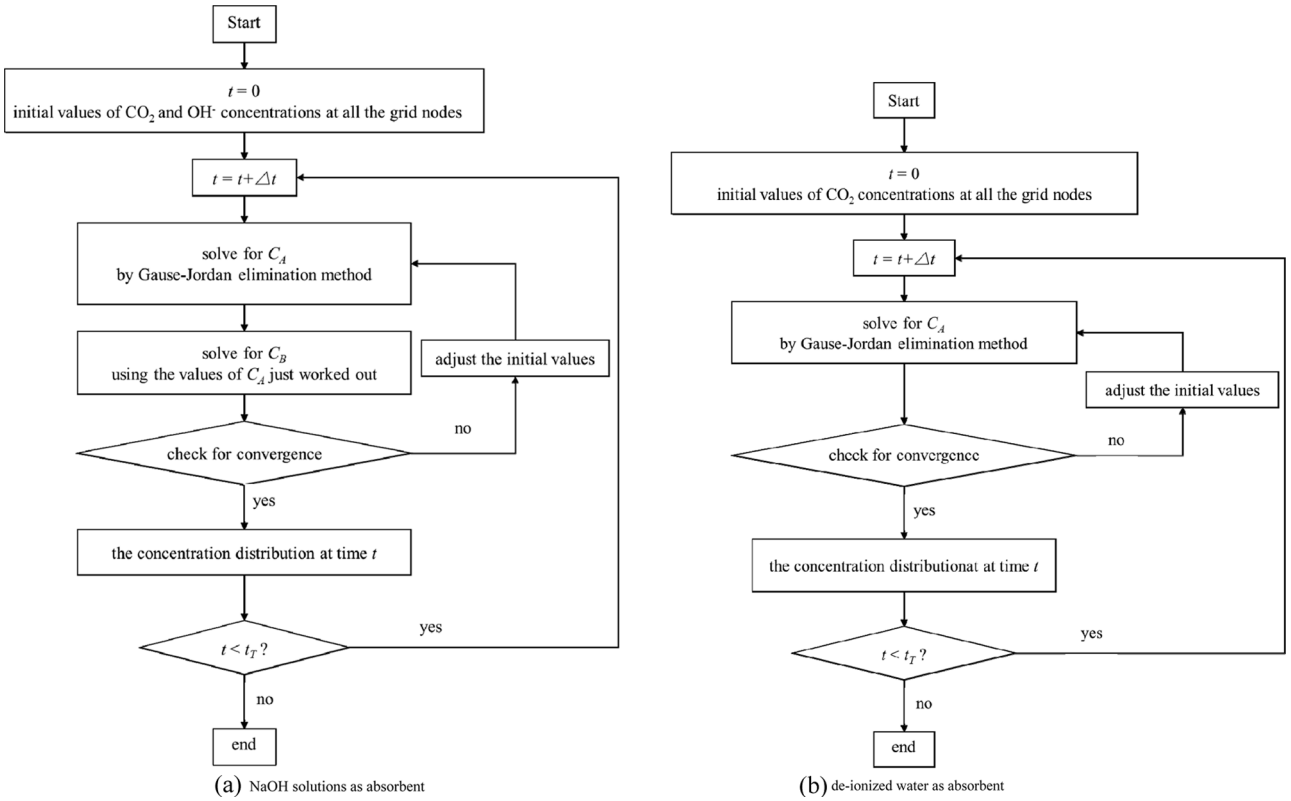

FIG. 3. Flow diagram for solving algebraic equations.

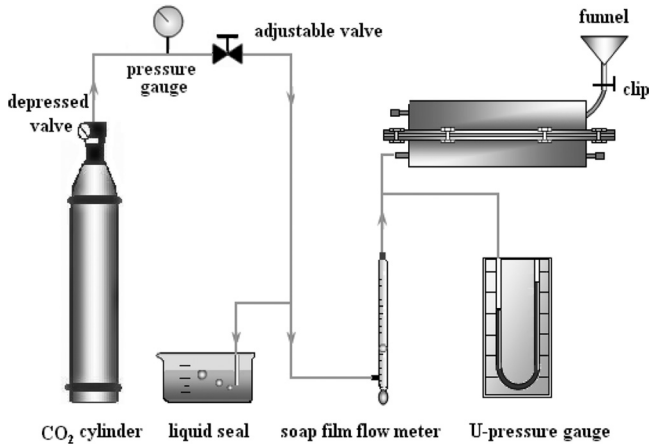

FIG. 4. Schematic diagram of experimental setup.

TABLE 1
Characteristic parameters of the flat-sheet membranes*

No.	Material	Pore radius** r_P (10^{-6} m)	Porosity***
1#	PTFE	0.178	79%
2#	PTFE	0.107	69%
3#	PTFE	0.204	52%
4#	PP	225	40%
5#	PP	180	30%
6#	PP	180	20%
7#	PP	180	12%

*PTFE membranes were provided by the Shanghai Lingflon Film Technology CO.LTD, and PP membranes were prepared in laboratory (boring by laser).

**PTFE membrane pore radiuses were measured by Coulter method, and PP membrane pore radiuses were measured from digital photo.

***PTFE membrane porosities were measured by dry/wet membrane method, and PP membrane porosities were measured from digital photo.

Modification for Actual Absorption Process

In the process of model calculation, the liquid phase is considered to be stagnant. However, it is hard to keep the liquid phase absolute immobility in the real practice. The gas pressure slightly fluctuates when the gas flows into the membrane contactor to keep a certain gas phase pressure, which can be observed by the U-pressure gauge in Fig. 4. The gas flow and pressure fluctuation may result in the disturbance in the liquid phase. Therefore, the real diffusion rate is higher than that in the stagnant liquid phase. And the enhancement factor of the diffusion coefficient is defined to modify the model results, as shown in Eq. (15):

$$E_l = \frac{D_l}{D} \tag{15}$$

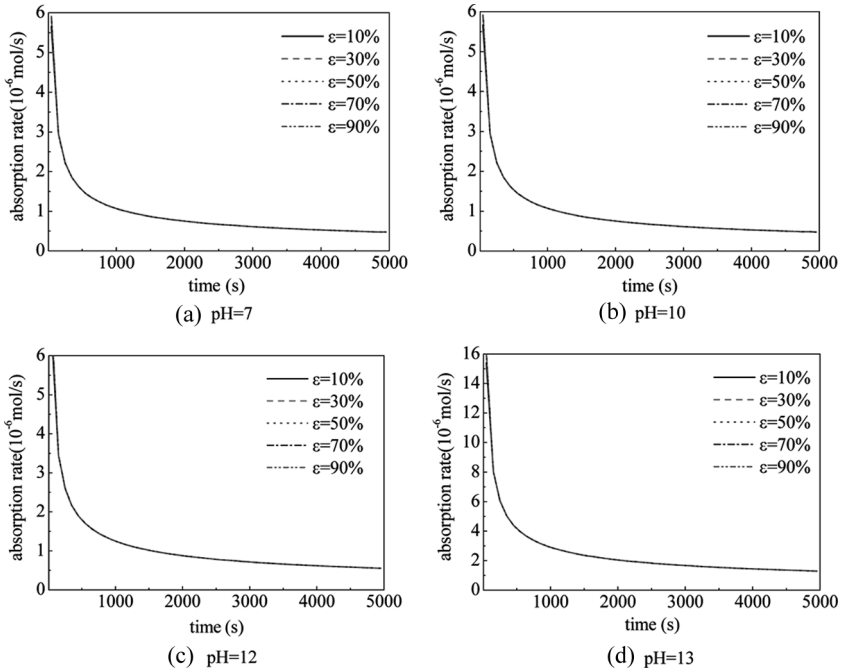

FIG. 5. Effect of membrane porosity on absorption rate at different pH values (when $r_P = 1.50 \times 10^{-6}$ m).

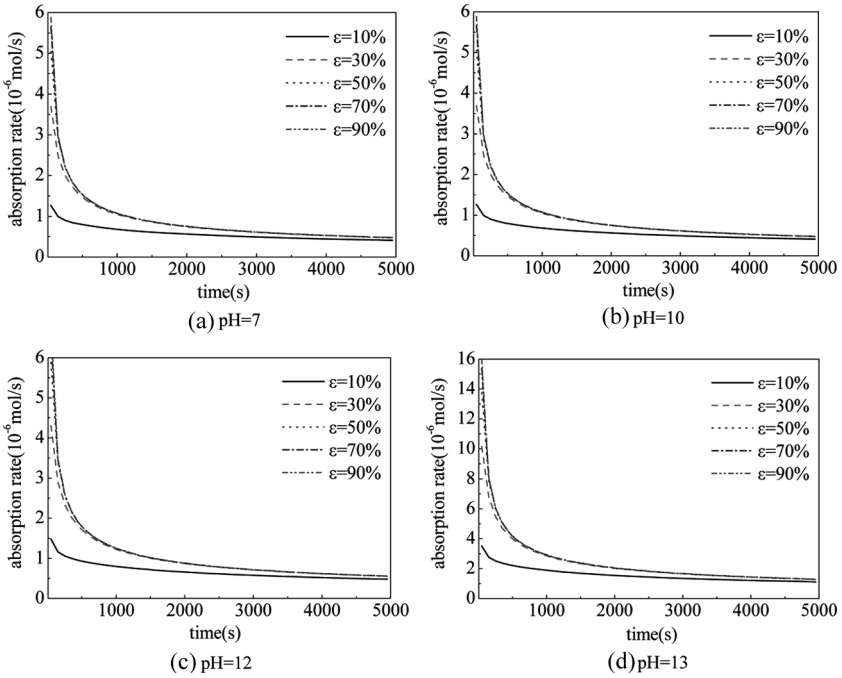

FIG. 6. Effect of membrane porosity on absorption rate at different pH values (when $r_P = 1.50 \times 10^{-4}$ m).

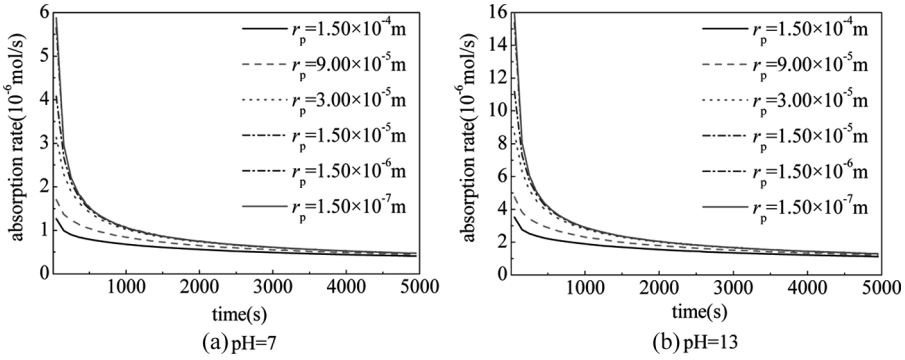

FIG. 7. Effect of pore radius on absorption rate (when $\varepsilon = 10\%$).

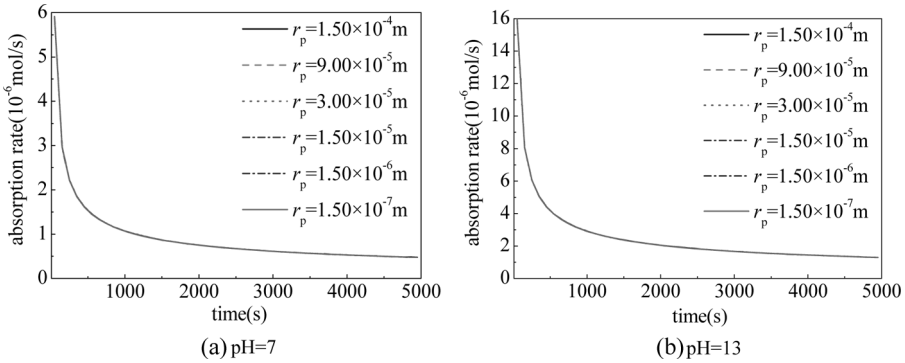

FIG. 8. Effect of pore radius on absorption rate (when $\varepsilon = 90\%$).

where D is the diffusion coefficient in the stagnant liquid phase; D_t is the diffusion coefficient in the disturbed liquid phase at time t.

According to the above analysis, the enhancement factor is related to the absorption rate. Therefore, it is defined as a function of the mass transfer driving force.

$$E_t = f(\Delta c) \tag{16}$$

$$\Delta c = c^* - \overline{c_l} \tag{17}$$

where c^* is the equilibrium CO_2 concentration at the gas/liquid interface; $\overline{c_l}$ is the average CO_2 concentration in the liquid phase.

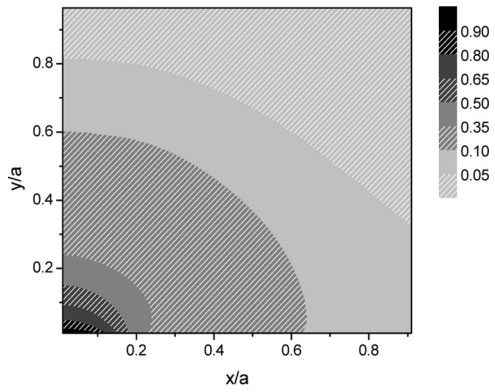

(a) $\varepsilon = 10\%$

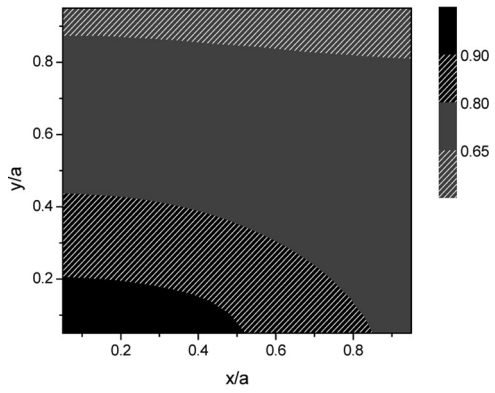

(b) $\varepsilon = 50\%$

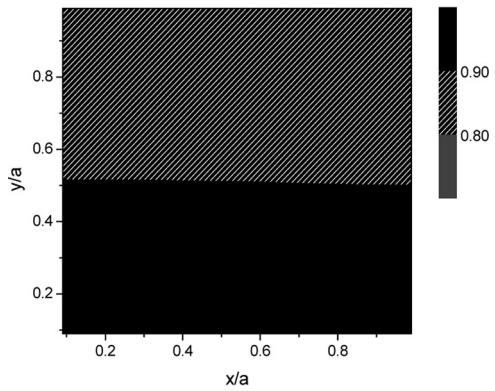

(c) $\varepsilon = 90\%$

FIG. 9. Effect of membrane porosity on the CO_2 concentration profile (c/c^*) ($r_P = 1.50 \times 10^{-4}$ m, absorbent pH = 7, $t = 150$ s).

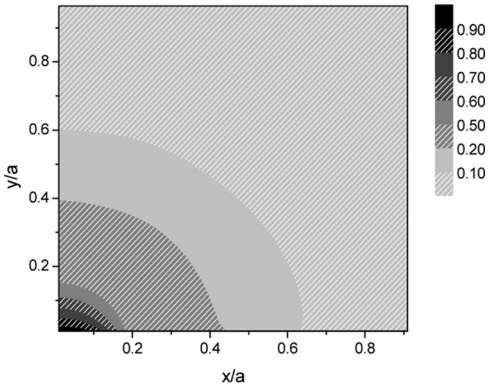

(a) $r_p = 1.50 \times 10^{-4} m$

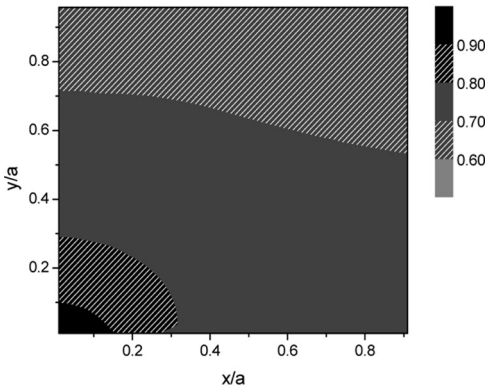

(b) $r_p = 1.50 \times 10^{-5} m$

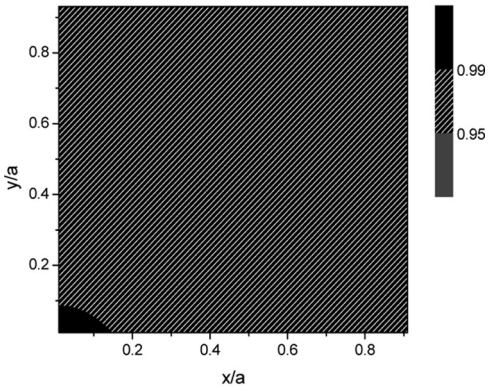

(c) $r_p = 1.50 \times 10^{-6} m$

FIG. 10. Effect of pore radius on the CO_2 concentration profile (c/c^*) ($\varepsilon = 10\%$, absorbent pH = 7, $t = 150$ s).

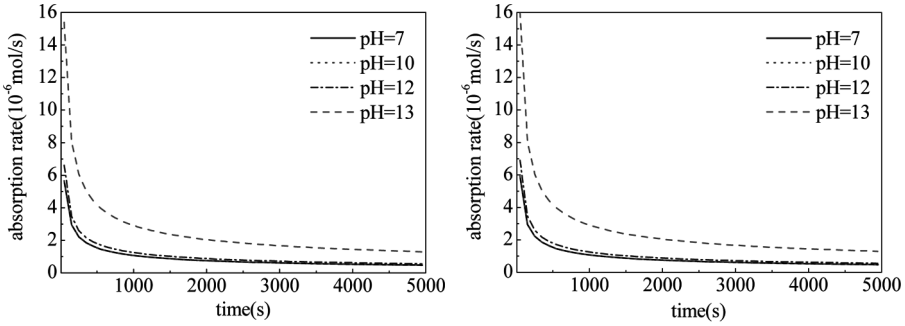

FIG. 11. Effect of absorbent pH value on absorption rate (when $r_p = 1.50 \times 10^{-6}$ m).

At the very beginning of the absorption process ($t = 0$), because of the motionless inertia of the liquid phase, the disturbance in the liquid phase is very small. And then the disturbance increases since the absorption rate at the initial time of the absorption process is relatively large. At last the disturbances smoothly down as the absorption rate descends with time. Therefore, the curve of $E_t = f(\Delta c)$ is a parabola.

EXPERIMENT

Pure CO_2 is absorbed by de-ionized water or NaOH aqueous solutions in a flat membrane contactor. The membrane contactor consists of two vessels with the same size of 300 mm length, 150 mm width, and 25 mm height. The membrane is placed between the two vessels and nylon wire meshes are used as support. The pH values of NaOH aqueous solutions are controlled by adjusting the concentration of NaOH, and the pH value is 7.4 when de-ionized water is used. The volume of the liquid absorbent is 1 L in all the experiments.

The experimental setup is shown in Fig. 4, and the characteristic parameters of the flat membranes are given in Table 1. In order to avoid the influence of the liquid flow, both the gas phase and the liquid phase are stagnant. Gas pressure is maintained constant by regulating the liquid seal. The absorption rate can be measured directly by the soap film flow meter.

RESULTS AND DISCUSSION

Model Results and Discussion

When the liquid phase is kept stable, the absorption rate decreases as the mass transfer driving force becomes smaller with the increasing CO_2 concentration in the liquid phase. The effects of membrane porosity on absorption rates at different pore radius and absorbent pH are shown in Figs. 5 and 6 respectively.

As shown in Fig. 5, the membrane porosity has less effect on the mass transfer process when the membrane pores are small ($r_P = 1.50 \times 10^{-6}$ m), and the absorption rate curves for different porosities are almost overlapped. According to Fig. 1, the distance between two adjacent pores is correspondingly small when the pore radius is small under constant porosity. The CO_2 layer soon fully covers the whole membrane surface in x direction. Therefore, the concentration profile near the membrane surface can achieve a comparatively homogeneous status easily, which means that the effect of porosity on the mass transfer process is not significant and the absorption rates at different porosities are nearly the same. On the contrary, when the pore size is large ($r_P = 1.50 \times 10^{-4}$ m), the concentration profile is hard to reach homogeneous within a short time. The effect of the membrane porosity on mass transfer is significant, which is shown in Fig. 6. Under this circumstance, the absorption rate increases with the increasing of porosity.

The effects of the pore size on the absorption rates at two different porosities are depicted in Figs. 7 and 8 respectively. It can be seen from Fig. 7 that the absorption rate increases with the decreasing membrane pore size at $\varepsilon = 10\%$. However, as shown in Fig. 8, the effect of the pore size on the mass transfer process becomes very small at $\varepsilon = 90\%$, and the absorption rate curves for different pore size are almost overlapped.

When the porosity is relatively small, the concentration profile near the membrane surface is inhomogeneous. In this case, the distance between two adjacent pores is sensitive to the change of the pore radius. The distance decreases obviously with the decreasing pore radius and the absorption rate increases. In this case, the change of the pore radius has a significant effect on the mass transfer process. When the membrane porosity reaches 90%, the pores on the membrane surface are very close to each other. The solute concentration profile near the membrane surface is relatively homogeneous. In such a case, the existence of the porous membrane has little effect on mass transfer, so the change of pore radius from 1.50×10^{-4} m to 1.50×10^{-7} m almost has no effect on the absorption rate.

It also can be seen from Fig. 6 that the effect of the porosity on mass transfer becomes less when the porosity is relatively large. There is an observable increasing of the absorption rate when the porosity increases from 10% to 30%, but the absorption rate curves for porosities 30%–90% are almost overlapped except for the absorption rate at the very beginning of the absorption process. A similar situation also can be observed in Fig. 7. When the pore radius is smaller than 3.00×10^{-5} m, the decreasing of the pore radius has less effect on the absorption rate. This can be attributed to the homogeneous concentration distribution near the membrane surface. When membranes with large porosities or small pores are applied, the solute concentration profile near the membrane surface can become homogeneous instantly due to the small distance between the adjacent pores. In this case, the continuously increasing of the porosity or the decreasing of the pore radius will have less effect on the absorbent rates.

The effects of membrane porosity and pore radius on the solute concentration profile near the membrane surface in the liquid phase are shown in Figs. 9 and 10 respectively. These two figures give the CO_2 concentration profiles above a pore when $t = 150$ s. Due to the symmetrical concentration profile above a pore, only half of the liquid region is plotted in Fig. 1(a). The abscissa represents the position above the pore in x direction, and is expressed by the dimensionless parameter x/a, where a is the distance between two adjacent pores as shown in Fig. 1. Similarly, the position in y direction is represented by y/a. The concentration contour values are labeled by c/c^* instead of the CO_2 concentration c. The concentration contour lines are not absolutely smooth because of the discretization in the calculation process.

According to the analysis above, as the distance between adjacent pores becomes smaller with the increasing porosity, the CO_2 concentration profile is getting more and more homogeneous when the porosity increases from 10% to 50%. However, beyond this range, the further increase of porosity does not keep this trend continuing since the concentration profile has become relatively homogeneous when the porosity is larger than 50%. Similarly, when the porosity is kept constant, the value of x/a does not change with the change of the pore radius, but the absolute value of the distance between adjacent pores becomes smaller with the decreasing pore radius. The solute concentration profile can get homogeneous more rapidly when the pore radius is smaller. Accordingly, the CO_2 concentration profile becomes much more homogeneous with the decreasing of pore radius from 1.50×10^{-4} m to 1.50×10^{-5} m. The effect of the pore radius on the mass transfer process is smaller when the pore radius decreases from 1.50×10^{-5} m to 1.50×10^{-6} m, because the distance between the adjacent pores has become small enough.

The effect of the absorbent pH on the absorption rate is shown in Fig. 11. It can be seen that the absorption rate increases with the increasing absorbent pH value. As the absorbent pH value increases, there are more OH^- ions in the liquid phase. Therefore, more CO_2 can be consumed by the chemical reaction, which results in a larger driving force of mass transfer and larger absorption rate. However, the increasing of the absorption rate is very low when

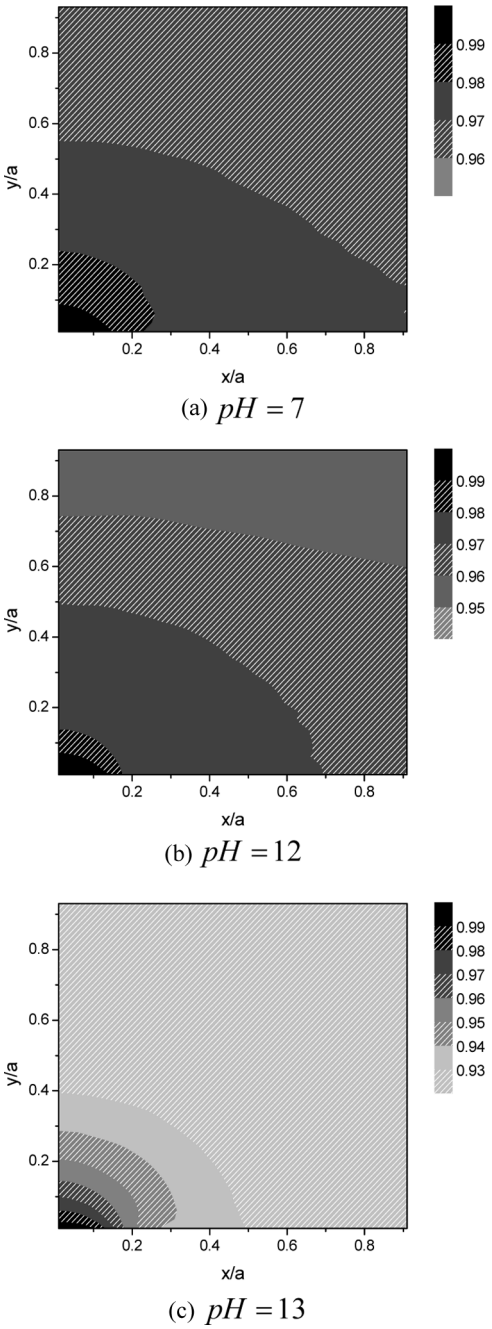

FIG. 12. Effect of absorbent pH value on the CO_2 concentration profile (c/c^*) $(r_P = 1.50 \times 10^{-6}\,\text{m}, \varepsilon = 10\%, t = 150\,\text{s})$.

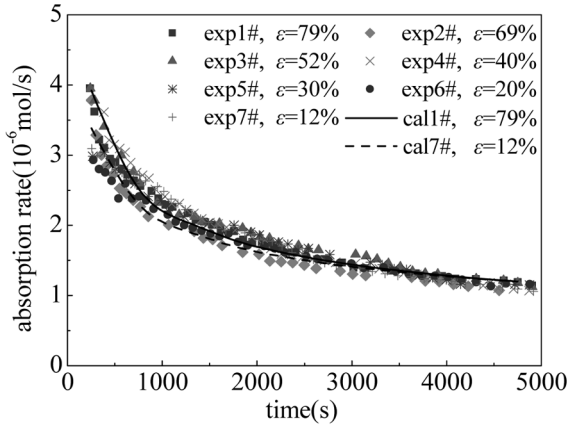

(a) pH=7

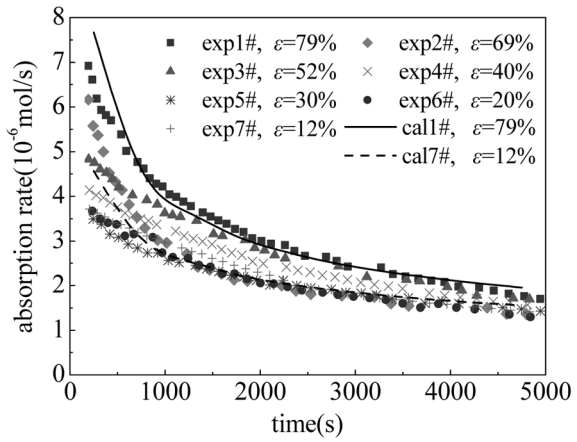

(b) pH=12

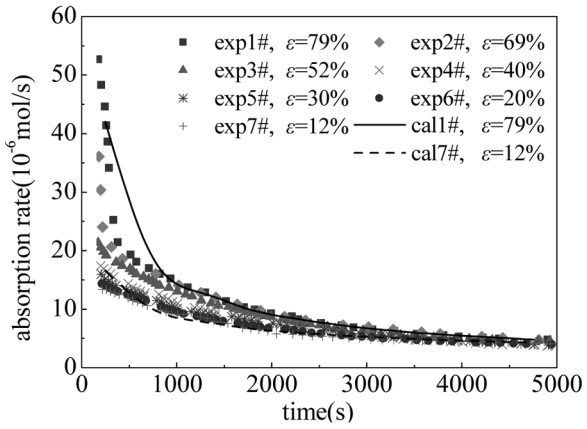

(c) pH=13

FIG. 13. Model results compared with experimental results.

$pH < 12$, because the OH^- concentration is still quite low in the liquid phase. Moreover, the chemical reaction makes it hard for the CO_2 layer to fully cover the whole membrane surface. The CO_2 concentration profile near the membrane surface is hard to get homogeneous as the absorbent pH value increases, which is shown in Fig. 12.

Matching Model Predictions with Experimental Results

In order to validate the model developed in this work, experimental data are employed to compare with the model results. Experimental results at pH 7, 12, and 13 are shown in Fig. 13. It can be found that the absorption rates using membranes with different porosities are almost the same at $pH = 7$, which means the porosity has less effect on the mass transfer process when the absorbent pH value is relatively lower. However, the absorption rate increases with the increasing porosity when the absorbent pH value increases to 12 or 13. In this case, the membrane porosity has a significant effect on the mass transfer process at relatively higher pH values. Absorption rate can be calculated by fitting the function of $E_t = f(\Delta c)$ and substituting it into the model. The model results are shown in Fig. 13 together with the experimental data. For the legibility of the figures, only the model results for membrane 1# ($\varepsilon = 79\%$, the largest porosity in this work) and 7# ($\varepsilon = 12\%$, the lowest porosity in this work) are plotted in Fig. 13. The model results agree well with the experimental data.

CONCLUSIONS

A theoretical model is developed to describe the mass transfer process when pure CO_2 is absorbed by de-ionized water or NaOH aqueous solution in a flat membrane contactor. The effect of the membrane structural characteristics is considered and numerical solutions are obtained by the finite volume method.

The effect of the membrane structural characteristics on the mass transfer in the liquid phase can be determined by the solute concentration distribution near the membrane surface. When membranes with relatively large porosity ($\varepsilon = 90\%$) or small pore ($r_P = 1.50 \times 10^{-6}$ m) are employed, the distance between the adjacent pores is small, so the solute concentration profile near the membrane surface in the liquid phase becomes homogeneous instantly. The effect of membrane structural characteristics on the mass transfer can be neglected in this case. On the contrary, when the membrane porosity is relatively small ($\varepsilon = 10\%$) or the pore size is large ($r_P = 1.50 \times 10^{-4}$ m), the distance between the adjacent pores is large, and correspondingly the solute concentration profile is inhomogeneous. Therefore the effect of the membrane structure characteristics is observable, and the absorption rate increases with the increasing porosity or the decreasing pore radius. However, once the concentration profile has achieved a relatively homogeneous status, continuous increasing of the porosity or decreasing of the pore radius has less effect on the mass transfer.

The absorption rate increases with the increasing of absorbent pH value. Due to the chemical reaction between CO_2 and OH^-, the increasing of the absorbent concentration makes it hard for the solute concentration profile near the membrane surface to become homogeneous.

The disturbance in the liquid phase caused by the gas flow and pressure fluctuation is further incorporated in the model. And the modified results agree well with the experimental results.

NOMENCLATURE

- a distance between adjacent pores as shown in Fig. 1 (m)
- c_A^* equilibrium concentration of CO_2 at the gas/liquid interface $c_A^* = 30\,\mathrm{mol \cdot m^{-3}}$
- c_A concentration of CO_2 in the liquid phase ($\mathrm{mol \cdot m^{-3}}$)
- c_B concentration of NaOH in the liquid phase ($\mathrm{mol \cdot m^{-3}}$)
- c_A^0 initial concentration of CO_2 in the liquid phase ($\mathrm{mol \cdot m^{-3}}$)
- c_B^0 initial concentration of NaOH in the liquid phase ($\mathrm{mol \cdot m^{-3}}$)
- D_A diffusion coefficient of CO_2 in the liquid phase ($\mathrm{m^2 \cdot s^{-1}}$)
- D_B diffusion coefficient of OH^- in the liquid phase ($\mathrm{m^2 \cdot s^{-1}}$)
- E_t enhancement factor of diffusion coefficient in liquid
- H Henry's constant of CO_2 ($\mathrm{mol \cdot m^{-3} \cdot Pa^{-1}}$)
- k_1 forward rate constant of the first step reaction between CO_2 and OH^- ($\mathrm{m^3 \cdot mol^{-1} \cdot S^{-1}}$)
- L thickness of the liquid phase (m)
- P pressure of the gas phase (Pa)
- r_P mean radius of micro-pore on the membrane (m)
- R_A reaction rate of CO_2 ($\mathrm{mol \cdot m^{-3} \cdot S^{-1}}$)
- R_B reaction rate of OH^- ($\mathrm{mol \cdot m^{-3} \cdot S^{-1}}$)
- t time (s)
- t_T overall absorption time (s)
- ε porosity of membrane

ACKNOWLEDGEMENTS

This work is supported by the National Natural Science Foundation of China (No. 20206002), the Program for New Century Excellent Talents in University (No. NCET-05-0122), and the Chinese Universities Scientific Fund (No. ZD0901).

REFERENCES

1. IPCC. (2002) *Climate Change 2001-The Science of Climate Change, Technical Summary of the Working Group I Report*; Cambridge University Press: Cambridge, U.K.
2. Wang, R.; Li, D.F.; Zhou, C.; Liu, M.; Liang, D.T. (2004) Impact of DEA solutions with and without CO_2 loading on porous polypropylene membranes intended for use as contactors. *J. Membr. Sci.*, 229 (1–2): 147–157.
3. Zhang, H.-Y.; Wang, R.; Liang, D.T.; Tay, J.H. (2006) Modeling and experimental study of CO_2 absorption in a hollow fiber membrane contactor. *J. Membr. Sci.*, 279 (1–2): 301–310.
4. Zhang, Q.; Cussler, E.L. (1985) Microporous hollow fibers for gas absorption: I. Mass transfer in the liquid. *J. Membr. Sci.*, 23 (3): 321–332.
5. Zhang, Q.; Cussler, E.L. (1985) Microporous hollow fibers for gas absorption: II. Mass transfer across the membrane. *J. Membr. Sci.*, 23 (3): 333–345.
6. Park, H.H.; Deshwal, B.R.; Kim, I.W.; Lee, H.K. (2008) Absorption of SO_2 from flue gas using PVDF hollow fiber membranes in a gas-liquid contactor. *J. Membr. Sci.*, 319 (1–2): 29–37.
7. Atchariyawut, S.; Jiraratananon, R.; Wang, R. (2008) Mass transfer study and modeling of gas-liquid membrane contacting process by multistage cascade model for CO_2 absorption. *Sep. Purif. Technol.*, 63: 15–22.
8. Lee, H.-K.; Jo, H.-D.; Choi, W.-K.; Park, H.-H.; Lim, C.-W.; Lee, Y.-T. (2006) Absorption of SO_2 in hollow fiber membrane contactors using various aqueous absorbents. *Desalination*, 200 (1–3): 604–605.
9. Kumar, P.S.; Hogendoorn, J.A.; Feron, P.H.M.; Versteeg, G.F. (2006) New absorption liquids for the removal of CO_2 from dilute gas streams using membrane contactors. *Chem. Eng. Sci.*, 57 (9): 1639–1651.
10. Versteeg, G.F.; Kuipers, J.A.M.; Van Beckum, F.P.H.; Van Swaaij, W.P.M. (1989) Mass transfer with complex reversible chemical reactions-I. single reversible chemical reaction. *Chem. Eng. Sci.*, 44 (10): 2295–2310.
11. Kim, Y.S.; Yang, S.M. (2000) Absorption of carbon dioxide through hollow fiber membranes using various aqueous absorbents. *Sep. Purif. Technol.*, 21 (1–2): 101–109.
12. Wickramasinghe, S.R.; Semmens, M.J.; Cussler, E.L. (1991) Better hollow fiber contactors. *J. Membr. Sci.*, 62 (3): 371–388.
13. Dindore, V.Y.; Brilman, D.W.F.; Versteeg, G.F. (2005) Modelling of cross-flow membrane contactors: Mass transfer with chemical reactions. *J. Membr. Sci.*, 255 (1–2): 275–289.
14. Dindore, V.Y.; Brilman, D.W.F.; Versteeg, G.F. (2005) Modelling of cross-flow membrane contactors: Physical mass transfer processes. *J. Membr. Sci.*, 251 (1–2): 209–222.
15. Evren, V. (2000) A numerical approach to the determination of mass transfer performances through partially wetted microporous membranes: Transfer of oxygen to water. *J. Membr. Sci.*, 175 (1): 97–110.
16. Keller, K.H.; Stein, T.R. (1967) A two-dimensional analysis of porous membrane transport. *Math. Biosci.*, 1: 421–437.
17. Malone, D.M.; Anderson, J.L. (1977) Diffusional boundary-layer resistance for membranes with low porosity. *AIChE J.*, 23 (2): 17.
18. Wakeham, W.A.; Mason, E.A. (1979) Diffusion through Multiperforate Laminae. *Ind. Eng. Chem. Fund.*, 18 (4): 301–305.
19. Versen, S.B.; Bhatia, V.K.; Dam-Johansen, K.; Jonsson, G. (1997) Characterization of microporous membranes for use in membrane contactors. *J. Membr. Sci.*, 130 (1–2): 205–217.
20. Li, J.L.; Chen, B.-H. (2005) Review of CO_2 absorption using chemical solvents in hollow fiber membrane contactors. *Sep. Purif. Technol.*, 41: 109–122.
21. Scovazzo, P.; Hoehn, A.; Todd, P. (2000) Membrane porosity and hydrophilic membrane-based dehumidification performance. *J. Membr. Sci.*, 167 (2): 217–225.
22. Supakorn, A.C.F.; Rong, W.; Ratana, J.; Liang, D.T. (2006) Effect of membrane structure on mass-transfer in the membrane gas-liquid contacting process using microporous PVDF hollow fibers. *J. Membr. Sci.*, 285 (1–2): 272–281.
23. Kreulen, H.; Smolders, C.A.; Versteeg, G.F.; van Swaaij, W.P.M. (1993) Microporous hollow fibre membrane modules as gas-liquid contactors Part 1. Physical mass transfer processes Aspecific application: Mass transfer in highly viscous liquids. *J. Membr. Sci.*, 78: 197–216.
24. Bhaumik, D.; Majumdar, S.; Fan, Q.; Sirkar, K.K. (2004) Hollow fiber membrane degassing in ultrapure water and microbiocontamination. *J. Membr. Sci.*, 235 (1–2): 31–41.
25. Wickramasinghe, S.R.; Semmens, M.J.; Cussler, E.L. (1992) Mass transfer in various hollow fiber geometries. *J. Membr. Sci.*, 69 (3): 235–250.

26. Rangwala, H.A. (1996) Absorption of carbon dioxide into aqueous solutions using hollow fiber membrane contactors. *J. Membr. Sci.*, 112 (2): 229–240.
27. Zhang, Z.T.; Gao, J.; Zhang, W.D.; Ren, Z.Q. (2006) Experimental study of the effect of membrane porosity on membrane absorption process. *Sep. Sci. Technol.*, 41 (14): 3245–3263.
28. Zhang, X.L.; Zhang, Z.T.; Zhang, W.D. (2005) Mathematical model of gas absorption for PTFE membrane and the effect of porosity. *J. Chem. Eng. Chin. U.*, 19 (4): 427–432.
29. Chen, G.; Ren, Z.Q.; Zhang, W.D.; Gao, J. (2007) Modeling study of influence of porosity on membrane absorption process. *Sep. Sci. Technol.*, 42 (15): 3289–3306.
30. Zhang, W.D.; Gao, J.; Shi, J.F. (2003) Concentration polarization of membrane absorption process of acidic gases. *Chin. J. Proc. Eng.*, 3 (4): 308–312.
31. Dorothy, A.; Jankowski, T.B.S. (1986). *Chemical Engineering Data Sources*; American Insitiute of Chemical Engineers.
32. Dankwerts, P.V.; Sharma, M.M. (1966) The absorption of carbon dioxide into solutions of alkalis and amines (with some notes on hydrogen sulfide and carbonyl sulfide). *Chem. Eng.*, 44: 244–279.
33. Versteeg, H.K.; Malalasekera, W. (1995) *An Introduction to Computational Fluid Dynamics The Finite Volume Method*; Longman Scientific & Technical: New York.